EFDA–JET–CP(08)04/17

M. Vrancken, A. Argouarch, T. Blackman, P. Dumortier, F. Durodié, M. Evrard,
R.H. Goulding, M. Graham, S. Huygen, Ph. Jacquet, A. Kaye, E.A. Lerche,
M.-L. Mayoral, M.P.S. Nightingale, D. Van Eester, M. Vervier
and JET EFDA contributors

Scattering-Matrix Arc Detection on the JET ITER-Like ICRHAntenna

Scattering-Matrix Arc Detection on the JET ITER-Like ICRHAntenna

M. Vrancken[1], A. Argouarch[2], T. Blackman[3], P. Dumortier[1], F. Durodié[1], M. Evrard[1], R.H. Goulding[4], M. Graham[3], S. Huygen[1], Ph. Jacquet[3], A. Kaye[5], E.A. Lerche[1], M.-L. Mayoral[3], M.P.S. Nightingale[3], D. Van Eester[1], M. Vervier[1]
and JET EFDA contributors*

JET-EFDA, Culham Science Centre, OX14 3DB, Abingdon, UK

[1]Association EURATOM-Belgian State, Laboratory for Plasma Physics, Royal Military Academy, B-1000 Brussels, Belgium
[2]Association EURATOM/CEA, CEA Cadarache, CEA/DSM/DRFC, F-13108, St.-Paul-lez-Durance, France
[3]EURATOM-UKAEA Fusion Association, Culham Science Centre, OX14 3DB, Abingdon, OXON, UK
[4]Oak Ridge National Laboratory, P.O. Box 20008, MS-6169, Oak Ridge, Tennessee, TN 37831-6169, United States
[5]ITER organisation, Building 519, F-13108, St.-Paul-lez-Durance, France
** See annex of M.L. Watkins et al, "Overview of JET Results ", (Proc. 21 st IAEA Fusion Energy Conference, Chengdu, China (2006)).*

Preprint of Paper to be submitted for publication in Proceedings of the 25th Symposium on Fusion Technology, Rostock, Germany
(15th September 2008 - 19th September 2008)

ABSTRACT

Operating Ion Cyclotron Resonance Heating (ICRH) antennas at high power density puts them at risk of arcing which reduces the coupled power to the plasma because the perturbed impedance match triggers the Voltage Standing Wave Ratio (VWSR) based generator trip system but even worse might damage the antenna beyond repair because of the the arc's localised energy deposition. New antennas are designed to operate in a load tolerant way which creates low impedance zones that are especially at risk since the existing VSWR protection systems are less sensitive to arcs in these areas. To protect these low impedance areas, a new arc protection system referred as Scattering Matrix Arc Detection (SMAD) was proposed. This paper describes the basic operating principle and implementation in hard- and software for the JET ITER-Like Antenna (ILA), with testbed and preliminary JET commissioning results.

1. INTRODUCTION

Operation of ICRH antennas in a regime where they couple high power to plasmas brings them close to their design limits in terms of voltage standoff, such that electrical breakdown or arcing is likely to occur, either plasma induced on the front Faraday screen or straps or at other high voltage locations inside the antenna or its feeding transmission lines. Such arc discharges are undesirable because they cause a malfunction of the antenna in terms of its impedance matching function between plasma load and generator and more seriously because the arcs localised energy dissipation can damage the antenna beyond repair.

Most existing arc detection schemes are based on measurement of the re ection or VSWR at the generator end of the feed transmission line and gives an overall protection of transmission lines and antenna by reducing the applied power by the generators low and fast enough (tripping of generator, typically within 10μs) to extinguish the arc.

However, this protection does not work for arcs that could occur at a low impedance location since these arcs will not result in any measurable additional re ection. Existing antennas (JET A2s [1]) and especially the new load-tolerant designs (JET-ILA [2], ITER ICRH launcher [3]) with a low-impedance T-point remain vulnerable to this danger.

The new proposed SMAD system (see Figure 1) relies on taking a sufficient set of RF measurements around the vulnerable area and an accurate RF model or S-matrix representation between the measurement points to perform a consistency check between the expected behaviour with-out arcs and the real measured behaviour (with or with-out arcs) of the antenna. In case of the ILA, the measurements are taken from two RF voltage pickup probes V_1, V_2 at the fixed strap end of each vacuum matching capacitor and the directional coupler forward and re ected voltages V_3^+, V_3^- on the feeding transmission line. The new SMAD scheme can thus protect the vacuum capacitors, the Vacuum Transmission Line (VTL) and the VaCuum Window (VCW) of the ILA,but not the plasma facing parts of the antenna nor the feeding transmission lines.

The SMAD will be used in parallel with the Subharmonic Arc Detection System (SHAD) [4],

[5] and existing VSWR system [6] to protect the antenna during JET operation and to study the occurence of arcs under ELMy H-mode plasma loading conditions.

The following Sections 2, 3 further detail the SMAD's principle of operation. Section 4 stresses the importance of accurate calibration of RF measurements and electronics to obtain a working arc detection system in practice. Section 5 describes the hardware used to obtain a fast calculation of the SMAD arc trip signal. First measurements from the ILA testbed are given in Section 6 while the first SMAD results from ILA commissioning on plasma are discussed in Section 7.

2. PRINCIPLE OF OPERATION

Figure 1 shows a simplified block diagram of one quarter of the ILA. The expected correct behaviour between the measurement points is stored in a Radio Frequency (RF) model in the form of a 3-port Scattering or S-matrix $S_{3\times3}$, determined by several S-matrices of parts of the antenna $S^{SCF}_{2\times2}$, $S^{VTL}_{3\times3}$, $S^{VCW}_{2\times2}$, derived from measurements or 3D electromagnetic simulations (see Section 3) and the capacitor values C_1, C_2.

The system of equations between V_1, V_2, V_3^+, V_3^- expressed with the components of $S_{3\times3}$ is overdetermined such that from the measurement of 3 quantities, the fourth can be predicted (assuming no arcs) as for example

$$V^-_{3calc} = K_1.V_{1meas} + K_2.V_{2meas} + K_2.V^+_{3meas} \tag{1}$$

and be compared with the actual measurement, giving a complex (amplitude and phase) error signal of the form

$$\Delta_1 = \frac{V^-_{3calc}\, V^-_{3meas.}}{V^+_{3calc}} = \Gamma_{calc} - \Gamma_{meas}. \tag{2}$$

In general, the system of equations can be solved for other quantities X of interest (which might exhibit higher sensitivities to arcs) and a general error formula of the form

$$K_1.X_1 + K_2.X_2 + K_3.X_3 + K_4.X_4 = 0 \tag{3}$$

can be programmed in hardware (see further Section 5), where all constants

$$K_i(S_{3\times3}(f), C_1, C_2, f), \qquad i = 1, \ldots, 4 \tag{4}$$

are determined by the RF model S-parameters S_{ij} (f), measured capacitor values C_1, C_2 and the operating frequency *f*. A complex boundary contour around the 0 error signal (or RF noise level) can be programmed as acceptable error before a trip signal is generated.

3. SCATTERING MATRICES FROM3D PHYSICAL MODELLING

At present, the RF model S-matrices for the ILA are derived from 3D electromagnetic simulations of parts of the antenna structure by CST Microwave Studio c [7]. Figure 2 shows a cross section of the ILA and how the structure is split into smaller parts for modelling purposes. A direct measurement verification of the $S_{3\times3}$ matrix would be desirable, but is not possible at present because measurement adaptors cannot be mounted once the antenna is assembled, while the weight of the inner VTL which is normally carried by the antenna straps and vacuum window cannot be carried by RF measurement adaptors alone. 3D simulation of the center VTL and back 30Ω line with vacuum window give the $S^{VTL}_{3\times3}$ and $S^{VCW}_{2\times2}$ S-matrices of Figure 1.

The front part $S^{SCF}_{2\times2}$ takes into account the moving Strokable Capacitor Flange (SCF) and a bellows. The S-matrices can be fit onto transmission line and lumped element cir- cuit models to analyse and predict the antenna behaviour. The voltage pickup probes are positioned at the strap end fixed capacitor anges as also shown in Figure 1.

4. RF AND ELECTRONICS CALIBRATION

The SMAD input signals V_1, V_2, V_3^+, V_3^- and C_1, C_2 are measured and processed as depicted in Figure 3. The RF signals are picked up by RF voltage probes and directional couplers on the antenna in the torus hall and brought to the RF plant over 117m long RF cables. The probe are split off into the ALM (Amplitude Limiting Module) to protect the capacitors from overvoltage, while the coupler signals are diverted to the SHAD electronics. The RFsignals are then downconverted and digitised by the Radio Frequency Conversion Module (RFCM) and Amplitude and Phase Detection Module (APDM) into 12 bit Amplitude and 10 bit Phase 0-10V DC output voltages that are put on a common digital bus. The digital signals are then read by the PXI (Peripheral Component Interconnect (PCI) eXtension for Instrumentation) real time processor to control the matching of the antenna [8] at a 5ms cycle time and separately by the SMAD PC for very fast 2μs arc detection calculations. The capacitor position potentiometer read back signals are analog 0-10V DC signals which are digitised in PXI and SMAD separately. Finally, the signals are also read by the central JET Control and Data Acquisition (CODAS) system and stored as slow (2.5ms) and fast (5.0μs) data in the JET Pulse Files (JPF).

For each of the sensors, cables and RF components, frequency dependent calibration data $S_{ij}(f)$ is stored. The RF probe calibration can be found in [9]. The directional coupler calibration measurements are depicted in Figure 4. The RFCM-APDM electronics were calibrated by injecting two amplitude and phase controlable RF signals and reading the digital outputs. The conversion appeared only slightly frequency dependent, such that the amplitude response could be linearised as

$$|V_k|_{DC} = a_k(f).|V_k|_{RF} + b_k(f) \tag{5}$$

while only the phase difference $\Delta\phi_{k,l}(f)$ between channels k and l needs to be stored. All calibration data is stored on the PXI hard drive and are used to display the data, but for the SMAD, the calibration

data is further combined and incorporated into the coefficients K_i of Equation (3) such that the SMAD hardware can calculate directly with the digital signals.

5. HARD- AND SOFTWARE IMPLEMENTATION

The SMAD system runs on a Linux PC with 4 dedicated PCI cards (one for each pair of straps or Resonant Double Loop (RDL) [2]) as depicted in Figure 5. The PCI cards can evaluate the error formula (Equation (3) or Equation (6) see further Section 6) and the logical functions to generate an arc trip signal very fast (cycle time 2μs) because they are programmed in hardware on a FPGA (Field Programmable Gate Array) and the input RF amplitude and phase signals are read directly from the common digital bus. Because the frequency is preset before a JET plasma discharge and the movements of the capacitors during the RF pulse are relatively slow (compared to the speed of an electrical arc event), the coefficients of the equation are calculated from stored tables and downloaded to the FPGA by the host PC only every 10ms as depicted in Figure 5. From the combined information of the SMAD, SHAD and VSWR trip signals, an overall arc protection system will have to defer the occurence of an arc and pass a resulting trip signal to the RF generator's Amplifier Trip Module (ATM). The precise functioning of the arc protection system can only be defined after evaluation of the different arc detection subsystems during the ILA commissioning on plasma.

6. TESTBED RESULTS

A first check of the RF model of the ILA was done on testbed by recording a set of V_1, V_2, V_3^+, V_3^- signals as the capacitors C_1, C_2 were moved over a square grid (in Figure 6) at 42MHz. These measurements were taken directly with a Network Analyser (without the automatic measurement chain of Figure 3). The initial mapping of the measured vs calculated error according to Equation (3) as in Figure 8 (a) prompted to rewrite the error formula as

$$\Delta_2 = \frac{K_1.V_{1meas.} + K_2.V_{2meas}}{V^-_{3meas.} - K_3.V^+_{3meas}} \qquad (6)$$

which indicates a systematic amplitude and phase error as seen in Figure 8 (b). After recalibration of the capacitor readback (o in Figure 6), and allowing a probe voltage amplitude correction of −15% and a -3^o on the phase of the forward and re ected directional coupler signals, the remaining errors could be reduced as shown in Figure 9 to a 15 to 20%level. With this level of modelling and measurement error (without arcs) remaining (indicated by dashed line circle in Figures 9 (b) and 7.), an inductor arc model with different values L is positioned at the conjugate T-point of the RF model, while the capacitors are moved again over the grid of Figure 6, which shows in Figure 7 that arcs up to 20nH should still be able to be detected.

7. JET COMMISSIONING RESULTS ON PLASMA

The SMAD model optimised from testbed is presently being tested as part of the general

ILAcommissioning phase [10]. At the moment of writing, the signal and calibration chain of Figure 3 is fully operational, but the SMAD hardware of Figure 5 is still being commissioned. However, all RF signals collected on the PXI controller and in the JPFs can be postprocessed after each RF pulse. The JET fast data calibration is presently available only in amplitude but is being completed for the phase as well for the complete set of signals.

Figure 10 shows SMAD relevant signals from the lower left RDL during JET pulse No. 73987 where the ILA matches and couples power into an L-mode and (type III) ELMy H-mode plasma at 42MHz. The change in measured capacitor voltage V_1, V_2 and forward and reflected V^+_{3meas}, V^-_{3meas} directional coupler voltages re ect the changing loading conditions on the antenna during the L- to H-mode transition starting at 13s and the ELMy H-mode from 13.3 to 15.6s. At the end of the pulse, around 15.5s, repeated VSWR tripping removes the applied RF power from the antenna. On the last trace, both SMAD error signals remain within the previously established 15 to 20% error band (despite the addition of RF and electronics noise).

There is a false error signal when the applied RF power is too low to be detected by the processing electronics at the start (11s) and end of the RF pulse(16s). Figures 11 zooms in on the VSWR and SMAD signals at the occurence of VSWR trips at the end of the pulse from 15.5 to 15.6s. The VSWR signals are collected in the JPF at 400Hz (slow) and 200kHz (fast) sampling rate.

The SMAD signal V^+_{3calc} is compared with the measured V^-_{3meas} signal in amplitude in phase at the PXI (slow) 200Hz sampling rate, and this shows that the error signals Δ_1, Δ_2 on the last trace remain stable despite the change in ELM loading conditions, except when the RF power is removed by the VSWR trip. The delay of the occurence of the VSWR trip with respect to the rise in the D_α signal and the fact that even bigger ELM excursions earlier in the pulse did not generate VSWR trips indicate that the ELMs are not causing these VSWR trips. When the fast data sampling (5μs JPF and 2μs SMAD) will be com- pletely available, the evolution of the SMAD signal during the RF trip power reduction (typically over 20μs) can be examined to conclude whether an arc has occured within the SMAD monitored region.

CONCLUSIONS

Low impedance areas of load-tolerant antennas need additional protection against occurence of electrical arcs under high power operating conditions. This paper has described the basic principles of the SMAD system that was proposed recently to achieve this goal. Its implementation in hard- and software on the JET ITER-Like Antenna has been described. Testbed and preliminary JET plasma commissioning results were presented. From present (mainly slow) data, it seems that an error signal is obtained that is stable under varying antenna load conditions and with a noise level smaller than the expected variation due to electrical arcs. With only the present data available, it is not yet possible to draw any conclusions on the ability to detect real electrical!ˇrcs. Further conclusions require fast data acquisition and testing of the SMAD under a larger variety of antenna operational circumstances (different frequencies, other matching configurations) and this further

work will lead to a combined use of the VSWR, SHAD and SMAD to allow safe operation of the ILA on JET.

ACKNOWLEDGEMENTS

This work was carried out within the framework of the European Fusion Development Agreement. The views and opinions expressed herein do not necessarily re ect those of the European Commission. The work carried out by UKAEA personnel was jointly funded by the UK Engi- neering and Physical Sciences Research Council and EURATOM.

REFERENCES

[1]. A. Kaye et al., "Present and Future JET ICRF Antenna," Fusion Engineering and Design, Vol. **24**, pp. 1-21, 1194.

[2]. F. Durodiee et al., "Main Design Features and Challenges of the ITER-like ICRF antenna for JET," Fusion Engineering and Design, Vol. **74**, pp. 223-228, 2005.

[3]. A. Borthwick et al, "Mechanical Design Features and Challenges for the ITER ICRH antenna," these proceedings.

[4]. F. Braun, "An ARC Detection system for ICR Heating," Proceedings of the 19th Symposium on Fusion Technology (SOFT), Lisbon, Portugal, September 16-20, 1996, pp. 601-603.

[5]. G. Berger-By et al., "Progress in Arc Safety System Based on Harmonics Detection for IRCH Antennae," Proceedings of the 17th Topical Conference on Radio Frequency Power in Plasmas, Clearwater, Florida, May 7-9, 2007, pp. 211-xxx, 2007.

[6]. I. Monakhov et al., "New Techniques for the Improvement of the ICRH System ELM tolerance on JET," Proceedings of the 15th Topical Conference on Radio Frequency Power in Plasmas, Moran, Wyoming, May 19-21, 2003, pp. 149-153, 2003.

[7]. CST GmbH, CST Microwave Studio c User Manual (2008).

[8]. M. Vrancken et al., "RF Measurements and Modeling from the JET ITER-Like Antenna Testing," Proceedings of the 17th Topical Conference on Radio Frequency Power in Plasmas, Clearwater, Florida, May 7-9, 2007, pp. 131-134, 2007.

[9]. M. Vrancken et al., "Recent ICRF Developments at JET," Proceedings of the 24th Symposium on Fusion Technology (SOFT), Warsaw, Poland, September 11-15, 2006, Fusion Engineering and Design, Vol. **82**, Issue 15-24, pp. 873-880, October 2007.

[10]. F. Durodié, "Commissioning on testbed of the ITER-Like ICRF Antenna for JET," these proceedings.

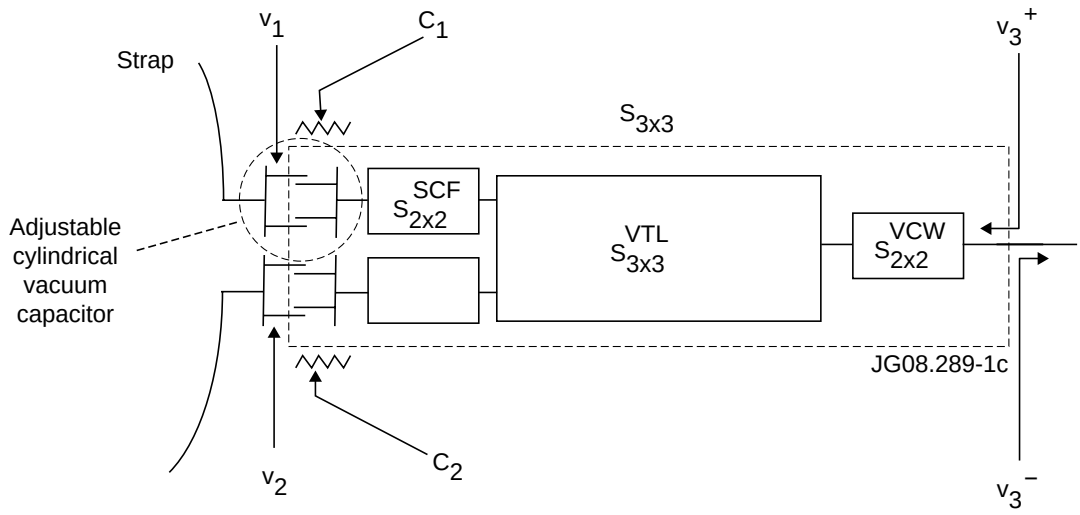

Figure 1: Schematic cross section of one quarter of the JET ILA with RF measurement points V_1, V_2, V_3^+, V_3^- and capacitor position readback C_1, C_2 used in SMAD arc detection.

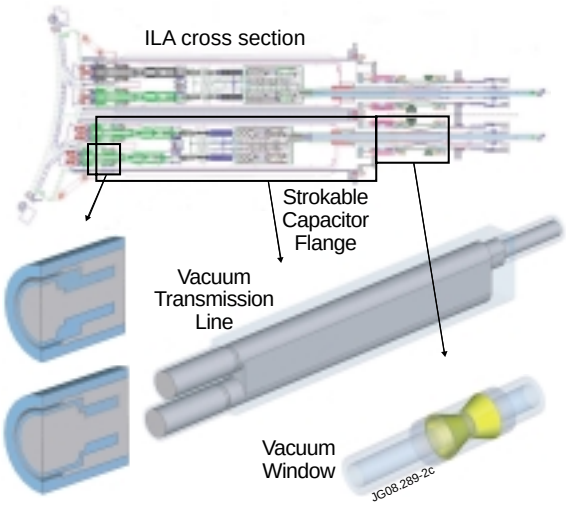

Figure 2: 3D electromagnetic physical modelling to extract SMAD 3 port Scattering matrix S_{3x3} and obtain a transmission line and lumped element antenna circuit model.

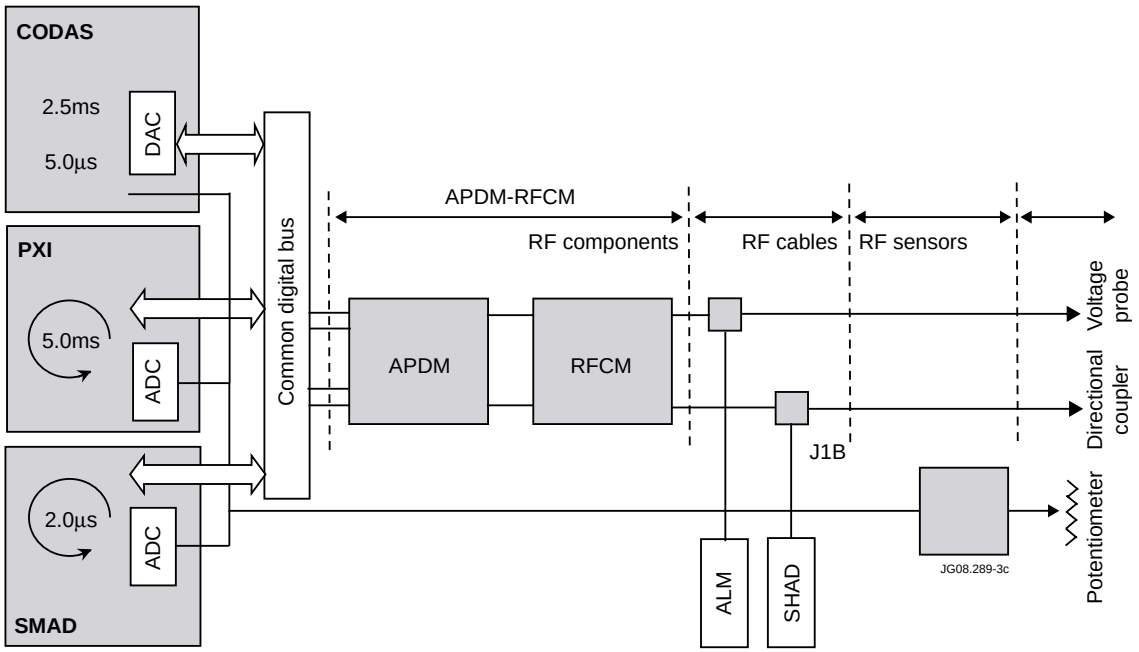

Figure 3: Signal flow chart with SMAD signals and required RF and electronics calibrations.

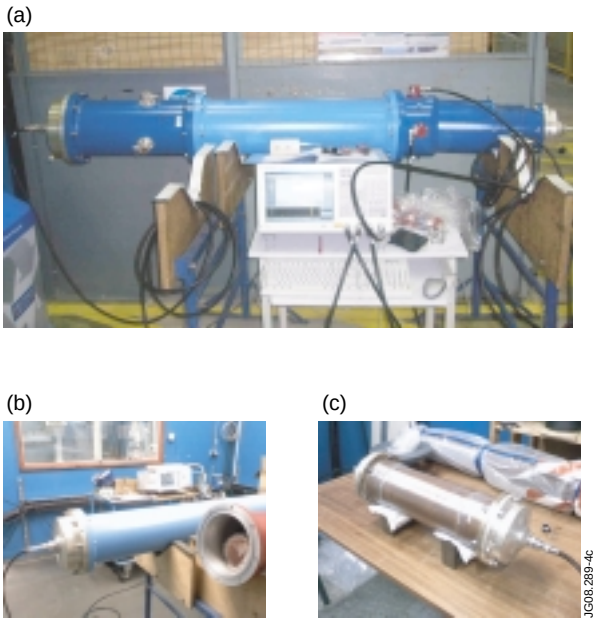

Figure 4: RF Calibration measurements for ILA directional couplers (a) and back to back measurements for characterisation of measurement adaptors (b),(c).

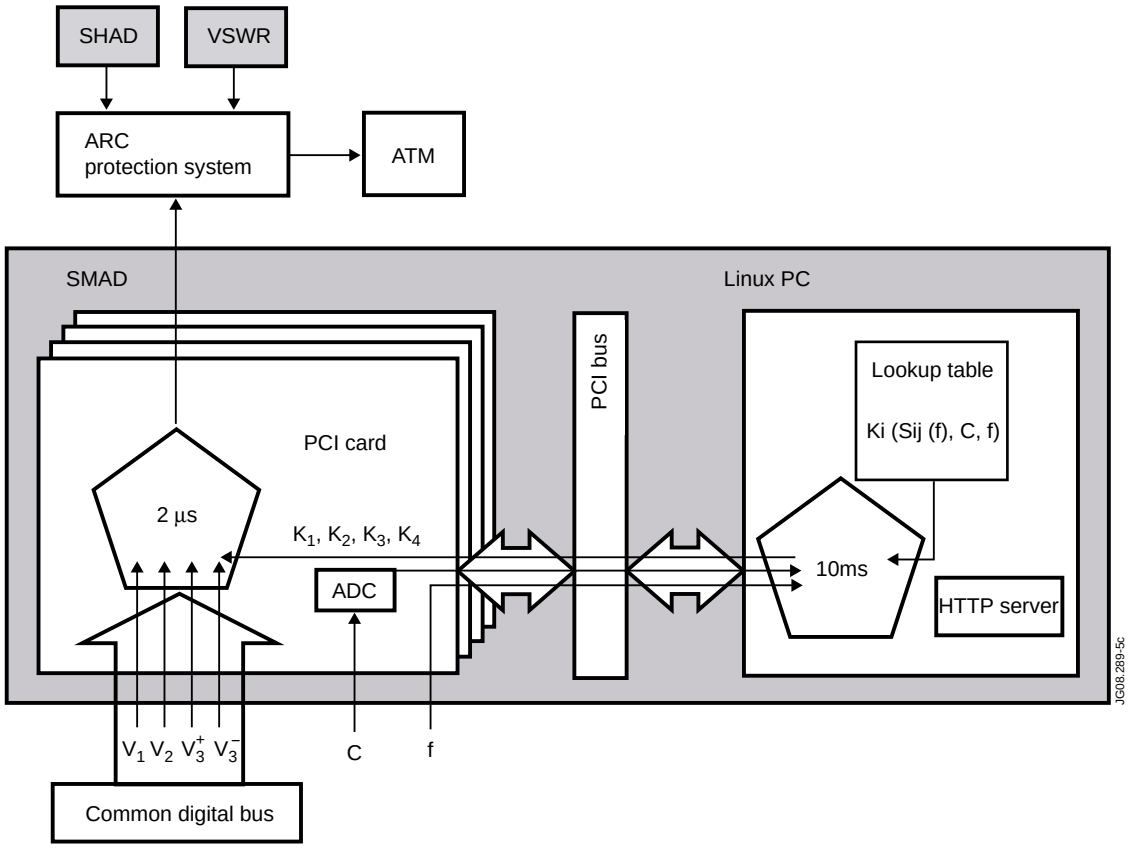

Figure 5: Flow chart of SMAD hard- and software and communication with other systems.

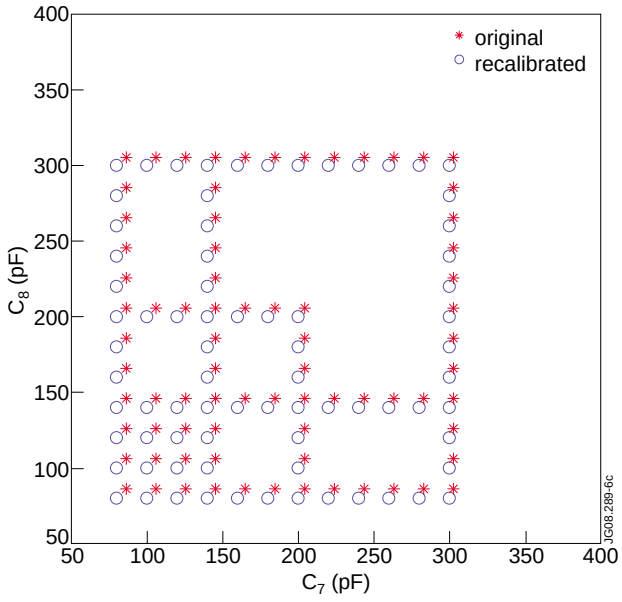

Figure 6: Original and recalibrated capacitor positions for measurement of probe and coupler signals.

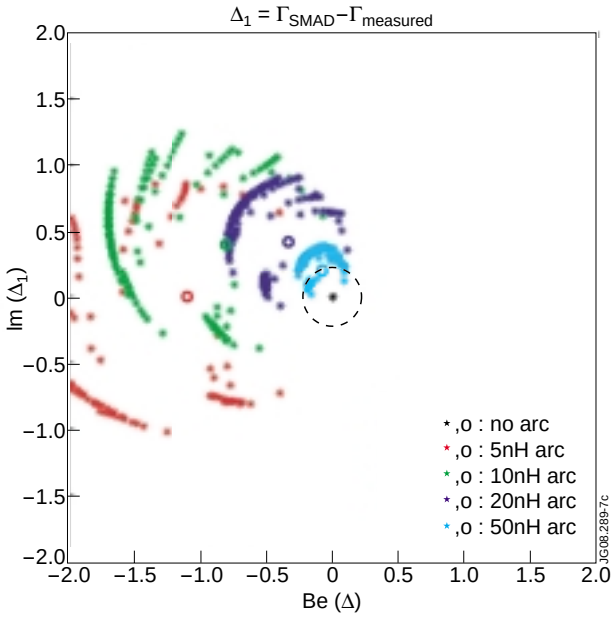

Figure 7: SMAD error signal Δ_1 as function of arc inductance L at 42MHz and 20% error circle.

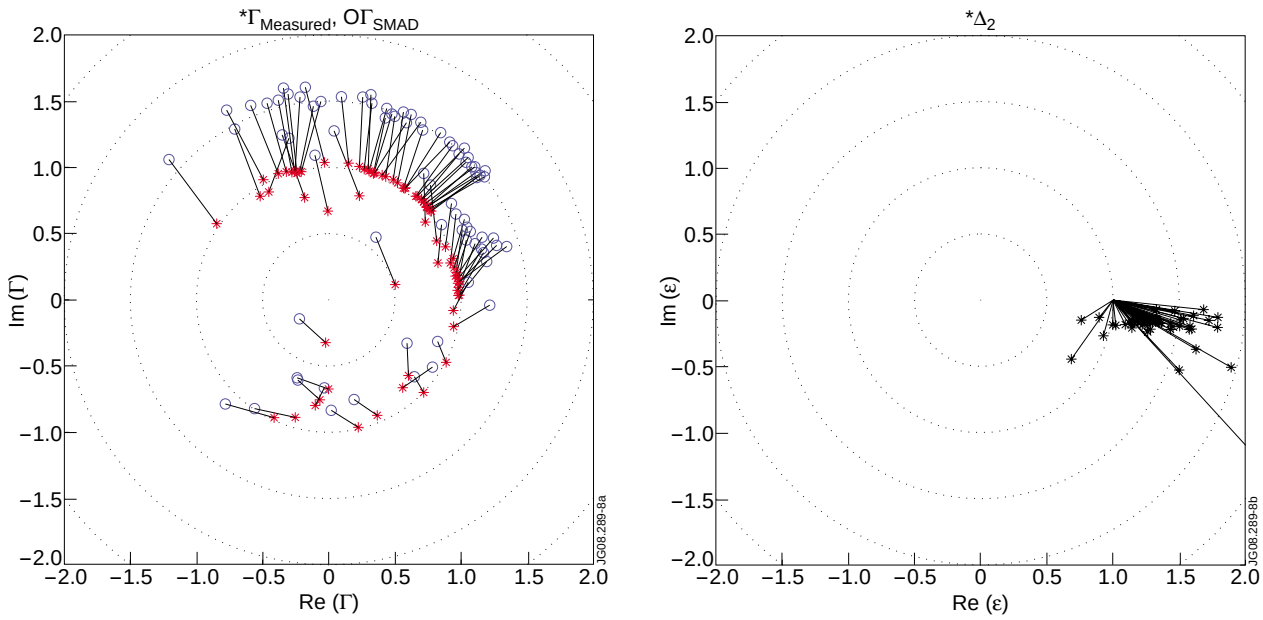

Figure 8: SMAD error signals from original testbed measurement.

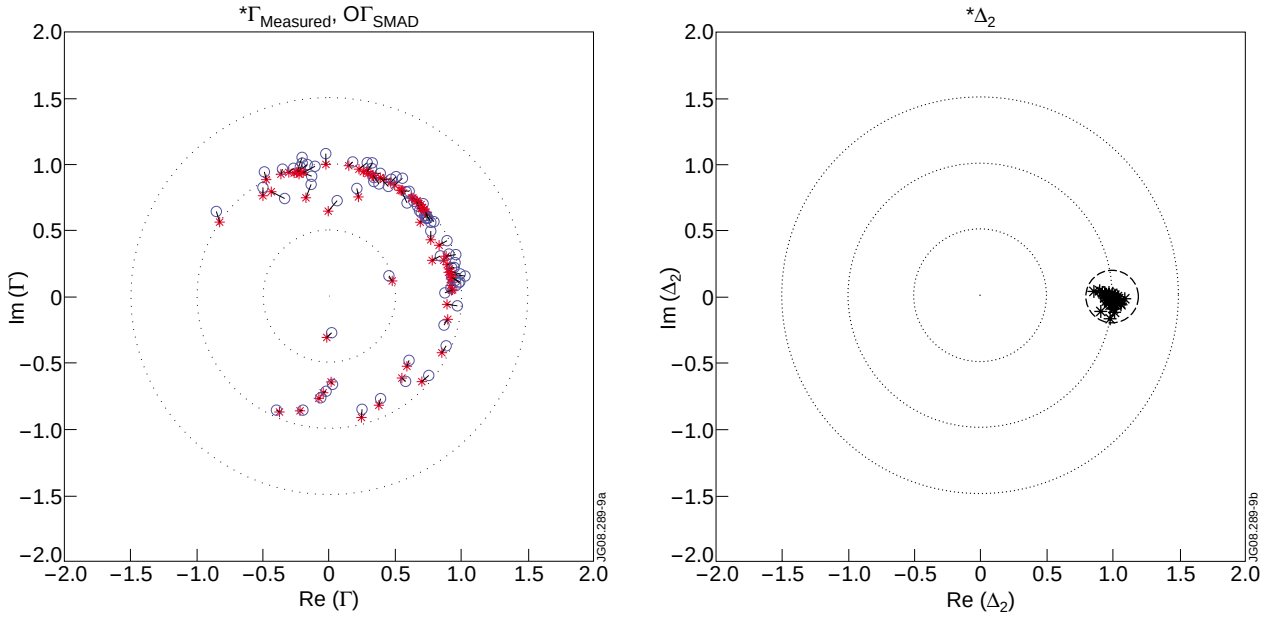

Figure 9: SMAD error signals after capacitor potentiometer recalibration and allowing curve fit on probe amplitude and directional coupler phase.

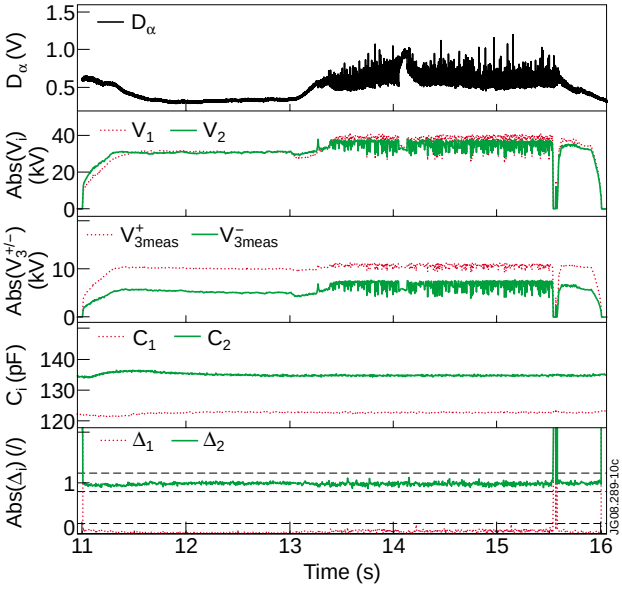

Figure 10: JET Pulse No. 73987 on L-mode and H-mode with type III ELM's, SMAD relevant D_α ELM signal, V_1, V_2 capacitor voltages,V_3^+, V_3^- forward and re ected voltages from directional couplers, C_1, C_2 capacitor readback input signals and Δ_1, Δ_2 SMAD error outputsignals with dashed line 20% error bands, at 42MHz from 11-16s.

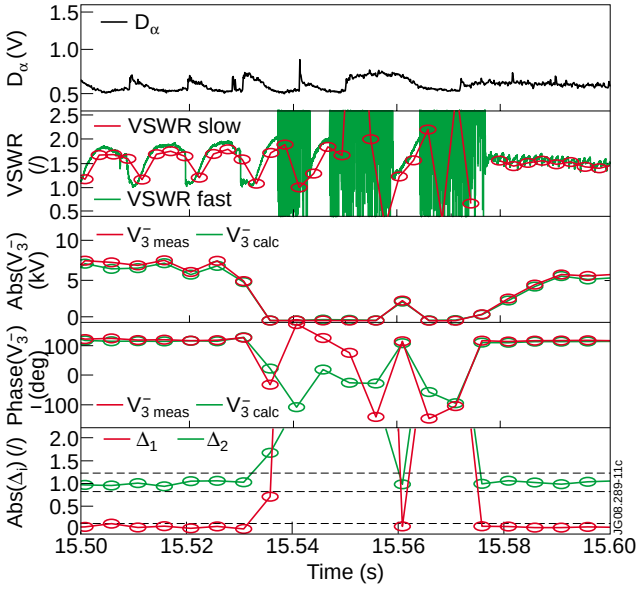

Figure 11: JET pulse No. 73987 time zoom with D ELM signal, VSWR slow and fast signals, V^-_{3meas}, V^+_{3calc} measured and SMAD calculated signals in amplitude and phase and 1, 2 SMAD error output signals at 42MHz from 15.5 to 15.6s